JOURNAL OF COMPUTATIONAL PHYSICS **138,** 449–479 (1997)
ARTICLE NO. CP975826

Flows in Forward Deformable Roll Coating Gaps: Comparison between Spring and Plane-Strain Models of Roll Cover

M. S. Carvalho and L. E. Scriven

Coating Process Fundamentals Program, Center for Interfacial Engineering and Department of Chemical Engineering & Material Science, University of Minnesota, Minneapolis, Minnesota 55455

Received October 8, 1996; revised May 30, 1997

Roll coating is distinguished by the use of one or more gaps between rotating cylinders to meter a continuous liquid layer and to apply it to a continuous flexible substrate. Of the two rolls that make a forward-roll coating gap, one is often covered by a layer of deformable elastomer. Thin films can be obtained without the risk of clashing two hard rolls. Liquid carried into the converging side of the gap can develop high enough pressure to deform the resilient cover, which changes the gap geometry and thus alters the velocity and pressure fields. The complete understanding of the flow in this situation is vital to the optimization of this widely used coating method; however, this elastohydrodynamic action is not well understood. The situation is similar to what is called the Soft-Elastohydrodynamic Lubrication regime (Soft EHL); however, the range of minimum distance between the rotating rolls, roll speed, and therefore flow rate through the gap in the roll coating process is one to three orders of magnitude larger than the typical values reported in previous work on Soft EHL. Earlier works on deformable roll coating analyzed the action with both the lubrication approximation and the full Navier–Stokes solution and different one-dimensional models of roll cover deformation. In order to test the accuracy of the past approaches, and to evaluate the relationship between the empirical constant used in the one-dimensional model to the relevant physical parameters, a complete, two-dimensional formulation has to be employed for both the liquid flow and the solid deformation. In this work, the flow between a rigid and a deformable rotating roll was examined by solving the complete Navier–Stokes system coupled with a non-linear plane-strain model of the roll cover deformation. The approximate and computationally cheaper approach is evaluated in which the compliant wall is represented by an array of radially-oriented Hookean springs. The equation system was solved by the Galerkin/finite element method; the

0021-9991/97 $25.00

resulting set of non-linear algebraic equations of the fully coupled problem was solved by Newton's method with initialization by pseudo-arc-length continuation as parameters were varied. Results show how roll deformation affects the total flow rate and forces on the rolls and illustrate how a deformable roll can be used to obtain thin coated layers with much less sensitivity to roll runout than those obtained with rigid rolls.

Key Words: deformable roll coating; liquid/solid interaction; non-linear deformation; free boundary problem; Galerkin's method.

1. INTRODUCTION

Roll coating processes are characterized by liquid flow in a narrow gap or nip between rotating cylinders or rolls. The liquid is metered and then applied to a continuous flexible substrate. Despite the variety of configurations, any such process can be broken into different parts [1]. In order to understand the whole process, one needs to study the individual flows between pairs of rolls in forward and reverse mode. Benjamin *et al.* [2] used simple mass balances to combine the information derived from the analysis of these *unit flows* between each pair of rolls in order to correlate the final film thickness (or coat weight) with roll separation and speed ratio at each roll pair in a system of rolls.

The flow between two rigid rolls has been extensively studied in the past [1, 3]. However, usually one of the rolls of each gap is covered with a resilient layer that deforms during operation. The main purposes of using a deformable roll cover are: (i) to avoid the risk of clashing two hard rolls; (ii) to meter much thinner films than ordinarily can be achieved by rigid roll coating; (iii) to reduce or delay the onset of the ribbing defect; and (iv) to transfer an already metered film. The deformation of the roll cover affects the shape of the boundaries of the coating flow. That flow generates pressure and viscous stresses, which tend to deform the roll cover. Hence, the viscous liquid flow and the deformation of the roll cover are coupled, which characterizes an *elastohydrodynamic action.* The main goal of theoretical analysis of the flow in a deformable roll coating gap is to determine the flow rate through the gap (that can be translated to a wet film thickness) as a function of roll speeds, roll position, and material properties.

A similar situation occurs in elastohydrodynamic lubrication [4] and more particularly in what is called soft elastohydrodynamic lubrication. Several theoretical models have been used to study this problem. In all of them, the liquid motion is described by Reynolds' equation of lubrication. Dowson and Higginson [4] adopted a simplified elastic deformation model (called the constrained column model), in which the deformation at each point is only a function of the pressure in that location. The same approach was adopted by Bennett and Higginson [5] to study the problem of a rotating steel cylinder loaded against a stationary plane covered with a deformable layer. Johnson [6] proposed that the proportionality constant on the one-dimensional model is a function of the Poisson's ratio ν, the elastic modulus E, and the layer thickness L, and it is given by

$$K \equiv \frac{P(x)}{\delta(x)} = \frac{(1-\nu)}{(1+\nu)(1-2\nu)} \frac{E}{L}.$$

It is clear that this expression cannot be used for incompressible materials, i.e., $\nu = 1/2$. Hooke [7] used a deformation model based on the asymptotic linear elastic solution of a compliant thin layer presented by Meijers [8]. The deformation in each point is a function of the entire pressure distribution. Dowson and Jin [9] compared the two deformation models and suggested that the constrained column model (one-dimensional model), with the proportionality constant proposed by Johnson [6], can be applied for Poisson's ratio less than 0.45 and for the ratio of loading width and layer thickness larger than 2. This result was expected, because when the proportionality constant proposed by Johnson [6] is used to model incompressible materials, the deformation at each point vanishes no matter how large the loading force. It is important to notice that the range of parameters at which these soft elastohydrodynamic solutions were obtained is very different from the operating conditions of deformable roll coating gaps: In the soft EHL examples presented, the compliant layer thickness was in the order of 1.5 mm, roll speed of 0.02 m/s, and film thickness in the order of 1 μm. In roll coating, the rubber cover thickness is in the order of 1 cm, roll speed varies typically from 1 to 10 m/s, leading to film thickness of 10 to 100 μm.

The thin elastic layers on soft elastohydrodynamic, deformable roll coating, as well as many other applications, are subjected to very large deformation. To give an accurate description of the deformation of the compliant layer, a complete two-dimensional finite deformation (non-linear elasticity) formulation has to be used. This was done by Batra [10], who analyzed the deformation of a rubber covered roll indented by a rigid cylinder. He used a Mooney–Rivlin constitutive equation to describe the behavior of the compliant layer. Bapat and Batra [11] extended the formulation for a non-linear viscoelastic constitutive equation. Oden and Lin [12] presented a formulation for the finite steady-state deformation of a rolling cylinder and solved the problem using a finite element method. These works were on dry contact between the cylinders, i.e., there was no liquid flow.

Coyle [13, 14] launched theoretical and experimental analysis of the elastohydrodynamics of roll coating. He approximated the behavior of a roll cover by a one-dimensional, linearly elastic model (the same approach used by Dowson and Higginson [4]), the behavior of the coating liquid by lubrication flow theory, and the film split region by Reynolds' condition. Carvalho and Scriven [15] took up Coyle's analysis and examined the differences between the use of one-dimensional linear and non-linear elastic models and two-dimensional plane-strain theory for which the deformable layer was regarded as an infinite elastic slab. They, too, approximated the flow in the coating gap by lubrication theory.

The lubrication approximation is not valid far from the region of closest approach between the rolls and near the free surfaces, where the flow is two-dimensional. To describe better the liquid flow in a coating gap, the full Navier–Stokes system of equations has to be solved. Carvalho and Scriven [16, 17] used the one-dimensional spring model coupled with the complete Navier–Stokes formulation for free-surface flows and linear stability analysis to study the three-dimensional stability limit of a film-split flow between a rigid and a deformable roll. The results obtained agree qualitatively with experimental evidences on the effect of rubber covered rolls on the behavior of the coating gap. However, two important issues are not

addressed: (1) What are the limitations of the simplified and computationally cheaper spring model? (2) What is the relation between the empirical spring constant and the rubber cover properties? Most roll cover materials are nearly incompressible rubber ($\nu \approx 1/2$). With this condition, the relation proposed by Johnson [6] cannot be used.

This work addresses these two important issues. The flow between rigid and a deformable rotating rolls fully submerged in a liquid pool is studied. Although this configuration does not represent a coating method, it does approximate well the flow in the gap region and it can be used to predict the flow rate through the coating gap. The flow is described by the complete Navier–Stokes system of equations. The deformation of the compliant roll cover is described by two different models: (i) independent, radially oriented springs that deform in response to the traction force applied at the extremity of each, i.e., the one-dimensional model used by previous researchers, and (ii) a plane-strain deformation of an incompressible Mooney–Rivlin material (non-linear elastic model). A Galerkin/finite element method is used to solve the system of differential equations. The resulting fully-coupled non-linear problem is solved by Newton's method, i.e., all the fields in the liquid and solid domain are solved simultaneously. With an appropriate initial guess, obtained here by pseudo-arc-length continuation, convergence could be achieved in four to five iterations.

Based on the flow rate predictions of both models, an empirical relation between the spring constant of the one-dimensional model and the roll cover thickness and elastic modulus is proposed.

2. DEFINITION OF THE SYSTEM

The liquid flow between a rigid roll and a deformable roll, both rotating and fully submerged in a pool is sketched in Fig. 1(a). Roll A is rigid and roll B is covered with a rubber layer. The roll surfaces move in the same direction in the gap region.

The nomenclature introduced by Coyle [13] is used here. If the center-to-center distance is larger than the sum of the roll radii, there is a clearance between the undeformed roll surfaces. Such situations are called *positive gaps.* If the center-to-center distance is smaller than the sum of the roll radii, the rolls would interfere were they undeformable. Such situations are called *negative gaps.* For convenience, both the *clearance* and the *interference* between undeformed rolls are called $2H_0$, as sketched in Fig. 1(b) and (c).

Each gap in a roll coater can be operated in two ways. One is to keep the axes of the two rolls parallel, with one axis fixed and the other movable in response to externally imposed loading. This is called a *load-controlled operation.* The other way is to fix the axes of both rolls. This is called a *fixed-gap operation.* In analysing roll coater gaps, it is convenient to suppose that the center-to-center distance between the rolls is set, and to evaluate the loading force required to maintain that distance. This tactic is used here, but it in no way limits the results to fixed-gap operation.

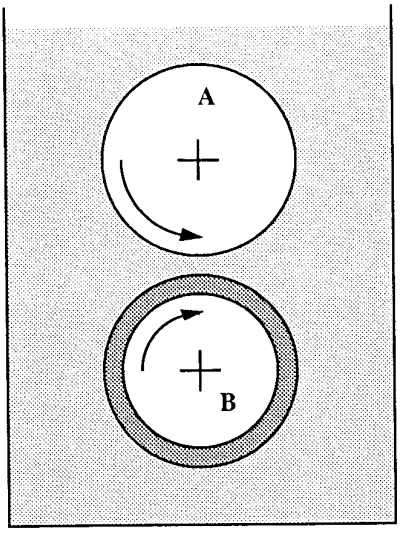

(a)

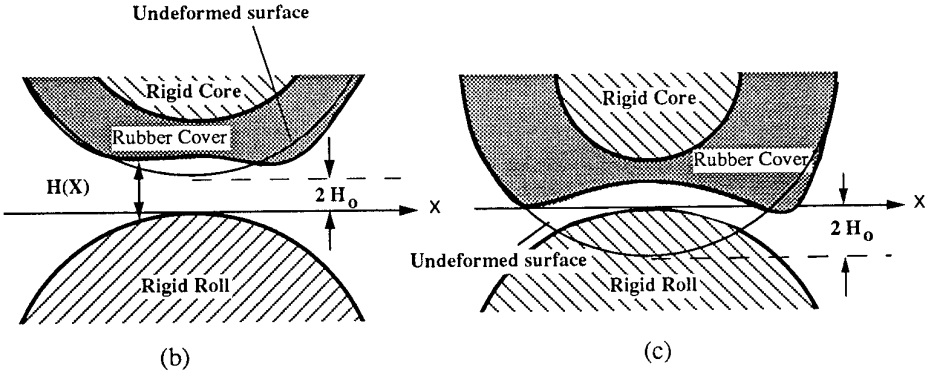

FIG. 1. (a) Sketch of flow between two rolls fully flooded in a liquid pool. (b) Detail of nip region in positive gaps; i.e., clearance of $2H_0$ between undeformed rolls. (c) Detail of nip region in negative gaps; i.e., interference of $2H_0$ between undeformed rolls.

2.1. *Equations of Liquid Flow*

The governing equations give rise to a *free boundary problem,* because the position of the deformable roll surface is unknown *a priori.* The basis of treating such problems is recounted briefly here. Fuller accounts were given by Kistler and Scriven [18, 19], Christodoulou and Scriven [20], and recently by Sackinger *et al.* [21].

Coating flows are laminar, and ideally steady and two-dimensional. The motion of the liquid is described by the Navier–Stokes equation and continuity equation of incompressible flow

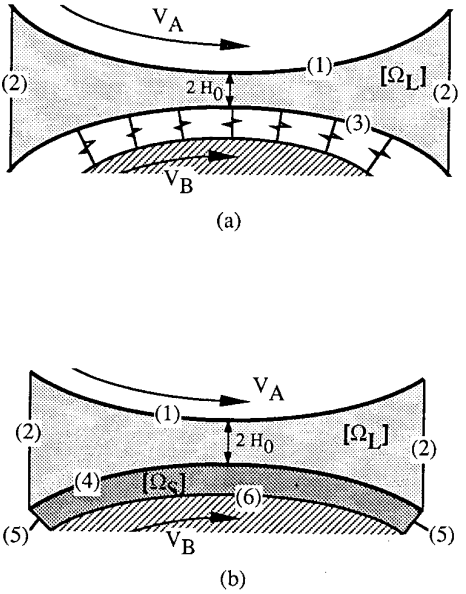

FIG. 2. Sketch of domains for flows between a rigid and a deformable roll fully submerged: (a) Spring model and (b) Plane-strain model.

$$\rho \mathbf{v} \cdot \nabla \mathbf{v} - \nabla \cdot \boldsymbol{\sigma} = 0 \qquad \text{and} \qquad \nabla \cdot \mathbf{v} = 0 \tag{1}$$

together with appropriate boundary conditions. ρ is the density of the liquid. $\boldsymbol{\sigma}$ represents the stress tensor (Cauchy stress tensor), the sum of pressure and viscous stress; for a Newtonian liquid it is,

$$\boldsymbol{\sigma} = -p\mathbf{I} + \mu(\nabla \mathbf{v} + (\nabla \mathbf{v})^T),$$

where μ is the liquid viscosity.

The deformation of the compliant roll cover is described by two different models, which are set out in Sections 2.3 and 2.4. The first model is a series of independent radially oriented springs. It is a simple approximation of the roll cover deformation. The main advantage is that the elastic response enters as a boundary condition on the liquid flow. The drawback of the complete description, i.e., the non-linear, plane strain formulation of the deformable wall, is that the deformation and velocity field of the entire roll cover have to be found, a considerably larger and more complex computation.

Figure 2 shows the domain of calculation. When the *spring model* (Fig. 2(a)) is used, there is only a liquid domain Ω_L. For the *plane-strain model* (Fig. 2(b)) there are a liquid domain Ω_L and a solid domain Ω_S.

At the rigid roll surface (1), the no-slip and no-penetration conditions apply, viz.,

$$\mathbf{v} = \mathbf{V}_{\text{Roll}} = \omega R \mathbf{t}, \tag{2}$$

where $\mathbf{t}$ is the unit tangent vector to the roll surface, in the direction of rotation; and ω is the angular speed of the roll, and R, its radius.

Along the inflow boundary and the outflow boundary (2), the pressure is assumed constant:

$$p = P_{\mathrm{IN}} \qquad \text{and} \qquad p = P_{\mathrm{OUT}}. \tag{3}$$

In the present analysis, both the inlet and outlet pressures were set to zero, although it could be instructive and useful to investigate the effects of pressure difference between the inflow and outflow sides. The inflow and outflow planes were positioned such that the total length of the domain analyzed was equal to the radius of the roll R. The theoretical predictions were virtually insensitive to moving the boundaries further away from the plane of the two roll centers.

The boundary conditions applied at the deformable roll surface (3) and (4) are discussed in Sections 2.3 and 2.4 for both the spring and plane strain models, respectively.

The liquid domain is unknown *a priori,* i.e., the shape of the deformable roll surface is part of the solution. In order to solve a free-boundary problem using standard techniques, the set of differential equations posed in the unknown domain Ω has to be transformed to an equivalent set defined in a suitable known reference domain Ω_0 (see Fig. 4). This is done by the mapping $\mathbf{x} = \mathbf{x}(\boldsymbol{\xi})$ that connects the two domains. Here the unknown physical domain is parametrized by the position vector $\mathbf{x}$, and the reference domain by $\boldsymbol{\xi}$, position in it. The reference domain adopted is to some extent arbitrary. A common approach in related coating flows has been to use a simple quadrangular domain tessellated into unit squares. That is done here.

The boundaries of the reference domain have to be continuously mapped onto the boundaries of the physical domain; and the mapping has to be invertible, i.e.,

$$\det(\nabla_{\boldsymbol{\xi}}\mathbf{x}) \neq 0 \qquad \text{for all } \boldsymbol{\xi} \in \Omega_0.$$

The gradient of the mapping $\nabla_{\boldsymbol{\xi}}\mathbf{x}$ at $\boldsymbol{\xi}$ in a two-dimensional domain is defined as

$$\nabla_{\boldsymbol{\xi}}\mathbf{x} \equiv \mathbf{J} = \begin{pmatrix} \dfrac{\partial x}{\partial \xi} & \dfrac{\partial y}{\partial \xi} \\ \dfrac{\partial x}{\partial \eta} & \dfrac{\partial y}{\partial \eta} \end{pmatrix},$$

where $|\mathbf{J}| \equiv \det(\mathbf{J})$ is the *Jacobian of the transformation.*

Spatial derivatives with respect to coordinates of the physical domain x and y can be written in terms of derivatives with respect to the coordinates of the reference domain ξ and η by using the inverse of the gradient of the mapping:

$$\begin{pmatrix} \dfrac{\partial \phi}{\partial x} \\ \dfrac{\partial \phi}{\partial y} \end{pmatrix} = \mathbf{J}^{-1} \begin{pmatrix} \dfrac{\partial \phi}{\partial \xi} \\ \dfrac{\partial \phi}{\partial \eta} \end{pmatrix}.$$

Area integrals over the physical domain are related by

$$d\Omega = |\mathbf{J}|\, d\Omega_0.$$

The construction of the mapping used in this work is discussed in the following section.

Both the modified set of differential equations that describe the velocity and pressure fields and the equations that define the mapping are solved by the Galerkin/finite element method on the reference domain Ω_0.

2.2. *Mapping from Physical to Reference Domain: Mesh Generation Scheme*

Finding a mapping that satisfies both requirements, viz., continuous mapping of boundaries and invertibility, is not always an easy task. Theoretical research on mesh generation addresses the issues of existence and uniqueness of such mappings [22–24]. The mapping used here is the one chosen earlier by de Santos [25]. It relies on elliptic partial differential equations to relate points of the physical domain to points of the reference domain. One way of choosing the differential equation that describes the mapping is to derive it from an extremum principle. This method consists of minimizing a functional that measures the departure from whatever mesh properties are deemed desirable, such as smoothness, orthogonality, and spacing.

de Santos [25] has shown that a functional of weighted smoothness can be used successfully to construct mesh for viscous free surface flows. The inverse of the mapping that minimizes the functional is governed by a pair of elliptic differential equations similar to the ones encountered in diffusional transport with variable diffusion coefficients. The potential of ξ-coordinate and that of η-coordinate satisfy the following equations:

$$\nabla \cdot [D_\xi \nabla \xi] = 0 \qquad \text{in } \Omega, \qquad \nabla \cdot [D_\eta \nabla \eta] = 0 \qquad \text{in } \Omega. \tag{4}$$

D_ξ and D_η are diffusion coefficients of coordinate potentials ξ and η. They control the spacing of whatever curves of constant ξ and constant η are chosen to tessellate the region into finite elements. The diffusion coefficients can be constructed in order to obtain a desired mesh spacing of curves at equal increments of one potential or the other.

Boundary conditions are needed in order to solve the second-order partial differential equations that describe the mapping from the reference domain to the physical domain. At the rigid roll surface, the shape and location of the roll were prescribed. The position of the deformable roll surface was implicitly defined by a force balance. The nodes were distributed along each boundary by means of distribution functions.

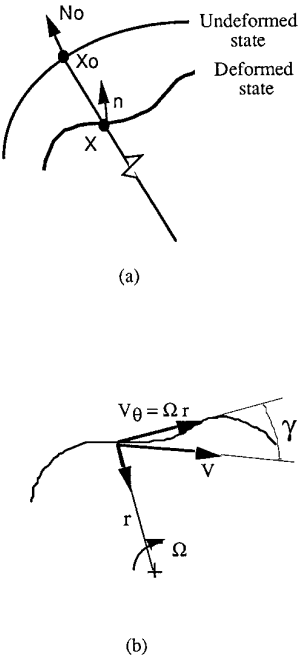

FIG. 3. Sketch of spring model: (a) deformation of the wall, (b) surface velocity.

2.3. *Spring Model of Deformable Walls*

A simple way of describing the deformation of a resilient wall is to assume that the displacement of each point on the undeformed wall is solely normal to the undeformed wall and depends on the loading at the location of that point on the deformed wall. Such a model amounts to a continuous distribution of independent springs oriented perpendicular to the undeformed wall, as sketched in Fig. 2(a). The disadvantages of this model are that it represents neither the shear stress that the liquid exerts, nor the incompressibility or limited compressibility (i.e., effects of the Poisson ratio) of the compliant wall.

In the Hookean version of this model, the displacement in the direction normal to the undeformed surface (radial direction in the case of cylindrical roll cover) is a linear function of the normal component of the hydrodynamic stress, as depicted in Fig. 3(a):

$$\mathbf{N}_0 \cdot (\mathbf{n} \cdot \boldsymbol{\sigma}) = -K \, \Delta X. \tag{5}$$

$\Delta X \equiv \mathbf{N}_0 \cdot (\mathbf{x} - \mathbf{X}_0)$ is the normal displacement of the wall; $\mathbf{X}_0$ is the position of a point on the wall in its undeformed state; $\mathbf{N}_0$ is the unit vector normal to the undeformed wall at $\mathbf{X}_0$; $\mathbf{n}$ is the unit normal vector to the deformed wall at $\mathbf{x}$; $\boldsymbol{\sigma}$ is the Cauchy stress tensor in the liquid, and K is the proportionality constant, referred to simply as spring constant, which is related to the elastic properties of the roll cover.

The loading force per unit area, or traction, that the liquid exerts on the resilient wall is $\mathbf{n} \cdot \boldsymbol{\sigma}$. If the liquid is Newtonian, the loading force is

$$\mathbf{n} \cdot \boldsymbol{\sigma} = -p\mathbf{n} + \mu \mathbf{n} \cdot [\nabla \mathbf{v} + (\nabla \mathbf{v})^T],$$

where p is the liquid pressure, and $\mathbf{v}$ its velocity.

The liquid velocity at a place on a compliant wall matches the velocity of the wall there, owing to the no-slip and no-penetration conditions. The velocity distribution along the surface of the deforming wall depends on how the wall is deforming. If as it moves, the wall deforms in such a way that its profile is steady, then its material velocity at every point is tangential. It is convenient to break its material velocity into two parts: a rigid-body motion, in particular the rigid rotation of the springs, which are arrayed radially around the axis of rotation; and a radial displacement motion that arises in the compression and expansion of the springs as they turn. The magnitude of the speed at each point is

$$V = \frac{V_{\text{Rig}}}{\cos \theta} = \frac{V_{\text{Rig}}}{\mathbf{n} \cdot \mathbf{N}_0}. \tag{6}$$

V_{Rig} is the component of the velocity that describes the rigid motion of the springs. For the case of radially oriented springs rotating at an angular speed of ω, $V_{\text{Rig}} \equiv \omega \times r$. Here $\mathbf{N}_0$ is the unit vector normal to the undeformed wall (radial direction in the particular case of rolls); $\mathbf{n}$ is the unit vector normal to the deformed wall at $\mathbf{x}$, as sketched in Fig. 3(b).

2.4. *Plane-Strain Deformation of Resilient Walls*

2.4.1. *Kinematic.* In order to describe fully the deformation of the roll cover, the current (deformed) configuration has to be compared with some convenient reference configuration (even if the roll cover never assumes that configuration). A natural choice is the configuration in which the stress tensor vanishes over the entire cover. This is called the *stress-free state.*

This work focuses on steady-states in which the deformation of no part of the material changes with time in the chosen ''laboratory'' frame of reference, even though the material is moving. A natural reference configuration for these states is the configuration assumed by the (deformable) wall when it is undeformed and moving as a rigid body. A useful example is Oden and Lin's [12] analysis of rolling dry contact. The location $\mathbf{X}$ in the reference configuration at a time t of the material particle that was at $\mathbf{X}_0$ in the reference configuration at $t = 0$ varies with time in a known manner: the *undeformed wall* by definition moves as a rigid body:

$$X = X(X_0, t), \qquad Y = Y(Y_0, t), \qquad Z = Z(Z_0, t).$$

The mapping $\mathbf{x} = \mathbf{x}(\mathbf{X})$ takes the reference configuration of the deformable wall (at time t) into the current (deformed) state of the wall (at the same time t). The velocity field of the deformable wall can be evaluated by differentiating the current position $\mathbf{x}$ of particle $\mathbf{X}_0$, i.e., $\mathbf{v} \equiv (\partial \mathbf{x}/\partial t)_{\mathbf{x}_0} = \mathbf{F} \cdot (\partial \mathbf{X}/\partial t)_{\mathbf{x}_0}$, where $\mathbf{F} \equiv (\partial \mathbf{x}/\partial \mathbf{X})$ is the deformation gradient tensor. In this relation, the cartesian components of velocity are related to the material coordinates by

$$u \equiv \left(\frac{\partial x}{\partial t}\right)_{\mathbf{x}_0} = \left(\frac{\partial x}{\partial X}\right)_t \left(\frac{\partial X}{\partial t}\right)_{\mathbf{x}_0} + \left(\frac{\partial x}{\partial Y}\right)_t \left(\frac{\partial Y}{\partial t}\right)_{\mathbf{x}_0} + \left(\frac{\partial x}{\partial Z}\right)_t \left(\frac{\partial Z}{\partial t}\right)_{\mathbf{x}_0}$$

$$v \equiv \left(\frac{\partial y}{\partial t}\right)_{\mathbf{x}_0} = \left(\frac{\partial y}{\partial X}\right)_t \left(\frac{\partial X}{\partial t}\right)_{\mathbf{x}_0} + \left(\frac{\partial y}{\partial Y}\right)_t \left(\frac{\partial Y}{\partial t}\right)_{\mathbf{x}_0} + \left(\frac{\partial y}{\partial Z}\right)_t \left(\frac{\partial Z}{\partial t}\right)_{\mathbf{x}_0}$$

$$w \equiv \left(\frac{\partial z}{\partial t}\right)_{\mathbf{x}_0} = \left(\frac{\partial z}{\partial X}\right)_t \left(\frac{\partial X}{\partial t}\right)_{\mathbf{x}_0} + \left(\frac{\partial z}{\partial Y}\right)_t \left(\frac{\partial Y}{\partial t}\right)_{\mathbf{x}_0} + \left(\frac{\partial z}{\partial Z}\right)_t \left(\frac{\partial Z}{\partial t}\right)_{\mathbf{x}_0}.$$

$(\partial X/\partial t)_{\mathbf{x}_0}$, $(\partial Y/\partial t)_{\mathbf{x}_0}$, and $(\partial Z/\partial t)_{\mathbf{x}_0}$ are defined by the rigid body motion of the wall when it is undeformed.

For the case of a deformable roll rotating at an angular velocity of ω, the velocity field on the rubber roll cover is evaluated as follows:

$$\begin{aligned} u &\equiv \left(\frac{\partial x}{\partial t}\right)_{\mathbf{x}_0} = \left(\frac{\partial x}{\partial X}\right)_t \left(\frac{\partial X}{\partial t}\right)_{\mathbf{x}_0} + \left(\frac{\partial x}{\partial Y}\right)_t \left(\frac{\partial Y}{\partial t}\right)_{\mathbf{x}_0} = -r\omega \sin(\phi + \omega t) = -Y\omega \\ v &\equiv \left(\frac{\partial y}{\partial t}\right)_{\mathbf{x}_0} = \left(\frac{\partial y}{\partial X}\right)_t \left(\frac{\partial X}{\partial t}\right)_{\mathbf{x}_0} + \left(\frac{\partial y}{\partial Y}\right)_t \left(\frac{\partial Y}{\partial t}\right)_{\mathbf{x}_0} = r\omega \cos(\phi + \Omega t) = -X\omega. \end{aligned} \tag{7}$$

2.4.2. *Equilibrium equations.* If the acceleration and body forces are negligible, the equilibrium equation in the current (deformed) configuration is simply

$$\nabla \cdot \boldsymbol{\sigma} = 0, \tag{8}$$

where $\boldsymbol{\sigma}$ is the Cauchy stress tensor. It is related to the deformation by an appropriate constitutive relation. In ordinary materials, the Cauchy stress tensor is a symmetric tensor. It pertains to the current configuration, and so it is said to be a true measure of the current state of stress. Hence it can be related only to a measure of deformation from the current configuration, for example by the left Cauchy–Green deformation tensor $\mathbf{B}$.

However, the deformed configuration is unknown *a priori;* in particular, finite roll cover deformation constitutes an inherently free boundary problem. Therefore, it is highly convenient to map the equation system of the deformed configuration to the known reference configuration so as to be able to use well-established methods of solving boundary value problems. To begin with, the equilibrium equation (8) has to be reexpressed in terms of quantities defined in the reference domain. This is accomplished by using Piola's transformation (see [26]), which is illustrated in the following sequence of tensor manipulations:

$$\int_{\Omega_S} \nabla \cdot \boldsymbol{\sigma}\, d\Omega = 0 \Rightarrow \int_{\Gamma_S} \mathbf{n} \cdot \boldsymbol{\sigma}\, d\Phi = 0$$

$$\Rightarrow \int_{\overline{\Gamma}} \mathbf{N} \cdot \mathbf{F}^{-1} \boldsymbol{\sigma}\, d\overline{\Gamma} = 0 \Rightarrow \int_{\overline{\Gamma}} \mathbf{N} \cdot \mathbf{T}\, d\overline{\Gamma} = 0 \Rightarrow \int_{\overline{\Omega}} \nabla_X \cdot \mathbf{T}\, d\overline{\Omega} = 0.$$

Ω_S and Γ_S are the area and the line boundary of the wall in its current (deformed) state. $\overline{\Omega}$ and $\overline{\Gamma}$ are the area and line boundary of the wall in the zero-stress configura-

tion that serves as the reference configuration. **n** and **N** are the outward unit normal vectors of the current and reference configurations, respectively.

Hence, the equilibrium equation in the reference domain becomes

$$\nabla_X \cdot \mathbf{T} = 0, \tag{9}$$

where $\mathbf{T} \equiv \mathbf{F}^{-1} \cdot \boldsymbol{\sigma}$ is the first Piola–Kirchhoff stress tensor. It is an asymmetric tensor.

It is relevant to point out here the difference between the reference domain Ω_0, introduced in Section 2.1 to solve the free boundary viscous flow problem there, and the zero-stress reference configuration $\overline{\Omega}$ used here, which also defines a reference domain. In the former, the reference domain is always a combination of quadrangular regions and is almost completely unrelated to the physics of the system. In the latter, the reference configuration does not need to be quadrangular, but it does need to be the zero-stress state, even if the body never assumes that configuration. de Almeida [27] and Sackinger *et al.* [21] have investigated the idea of using stress-free states and deformations of them in hypothetical elastic materials to generate reference states for free boundary flows.

The loading responsible for the solid deformation is the liquid traction. At the interface between solid and liquid the traction vectors exerted by each on the other must balance:

$$\mathbf{N} \cdot \mathbf{T} = -\mathbf{n}_l \cdot \boldsymbol{\sigma}_l = p\mathbf{n}_l - \mu \mathbf{n}_l \cdot [\nabla \mathbf{v} + (\nabla \mathbf{v})^T]. \tag{10}$$

N is again the outward unit normal vector in the zero-stress configuration of the solid, **T** is the first Piola–Kirchhof stress tensor, $\mathbf{n}_l$ is the outward unit normal vector of the liquid domain, and $\boldsymbol{\sigma}_l$ is the (Cauchy) stress in the liquid.

In order to find the current state of the deformed wall **x**, the stress tensor has to be related to a measure of deformation by a constitutive equation.

2.4.3. *Constitutive equation.* As pointed out in the previous section, any strain measure to which the Cauchy stress tensor is to be related needs to pertain to the current configuration. For an isotropic elastic solid the most general representation is [26]

$$\boldsymbol{\sigma} = f(\mathbf{B}) = f_0(I_B, II_B, III_B)\mathbf{I} + f_1(I_B, II_B, III_B)\mathbf{B} + f_2(I_B, II_B, III_B)\mathbf{B}^{-1}.$$

I_B, II_B, and III_B are the invariants of the left Cauchy–Green tensor **B**.

If the solid is incompressible, the third invariant is equal to unity ($III_B = 1$), and the foregoing expression simplifies to

$$\boldsymbol{\sigma} = -\pi\mathbf{I} + \beta_0(I_B, II_B)\mathbf{B} + \beta_1(I_B, II_B)\mathbf{B}^{-1}.$$

If the coefficients β_0 and β_1 are constant, this reduces to the equation of the Mooney–Rivlin material, a model of certain elastomers:

$$\boldsymbol{\sigma} = -\pi\mathbf{I} + \beta_0\mathbf{B} + \beta_1\mathbf{B}^{-1}. \tag{11}$$

If $\beta_1 = 0$, the constitutive relation reduces to what is called neo-Hookean material or ideal elastomer:

$$\boldsymbol{\sigma} = -\pi\mathbf{I} + \beta_0\mathbf{B}.$$

π is a scalar, pressure-like function that is related to the incompressibility constraint $III_B = 1$ (just as pressure in an incompressible liquid is related to the equation, or constraint, $\nabla\cdot\mathbf{v} = 0$).

The roll cover is generally very wide compared to its thickness. If the side effects are disregarded, the roll cover is in a plane-strain deformation state, i.e., the deformation in the transverse direction vanishes and the derivatives of all quantities in that direction also vanish:

$$z = Z \qquad \text{and} \qquad \frac{\partial(*)}{\partial Z} = 0.$$

Batra [10] showed that in the plane-strain deformation, the displacement and the Cauchy stress components in the X–Y plane of a Mooney–Rivlin material depend on the material constants β_0 and β_1 through their difference $\beta_0 - \beta_1$ alone. Therefore, the response of a neo-Hookean material is the same as that of a Mooney–Rivlin one, provided the coefficient β_0 used in the neo-Hookean equation is equal to the difference between β_0 and β_1 used in the Mooney–Rivlin equation.

Because the equation system is solved in the reference domain, the appropriate equilibrium equation to be used is Eq. (9). Consequently, the first Piola–Kirchhoff stress tensor of a Mooney–Rivlin material, Eq. (10), has to be evaluated. This is done by simply premultiplying the Cauchy stress tensor by the inverse of the deformation gradient tensor:

$$\mathbf{T} \equiv \mathbf{F}^{-1}\cdot\boldsymbol{\sigma} = -\pi\mathbf{F}^{-1} + \beta_0\mathbf{F}^{\mathbf{T}} + \beta_1\mathbf{C}^{-1}\cdot\mathbf{F}^{-1}.$$

This expression, with $p^* \equiv \pi - 3\beta_1$, can be rewritten as

$$\mathbf{T} = -p^*\mathbf{F}^{-1} + \beta_0\mathbf{F}^{\mathbf{T}} - \beta_1[\mathrm{tr}(\mathbf{C})\mathbf{F}^{\mathbf{T}} - \mathbf{C}\cdot\mathbf{F}^{\mathbf{T}}], \tag{12}$$

where $\mathrm{tr}(\mathbf{C})$ is the trace of the right Cauchy–Green deformation tensor; and p^* is a new pressure-like scalar function that relates to the incompressibility equation $III_C = 1$. It can be written in terms of the pressure p in Mooney–Rivlin material, which is incompressible:

$$p^* = p + \beta_0 - 2\beta_1.$$

From another point of view the incompressibility equation is a ''constraint'' and p^* is a ''Lagrange Multiplier.''

In this approach, the displacements and hence the positions of material points throughout the deformed roll cover are calculated, in contrast to the spring model, where only the radial displacements of points at the solid/liquid interface are computed.

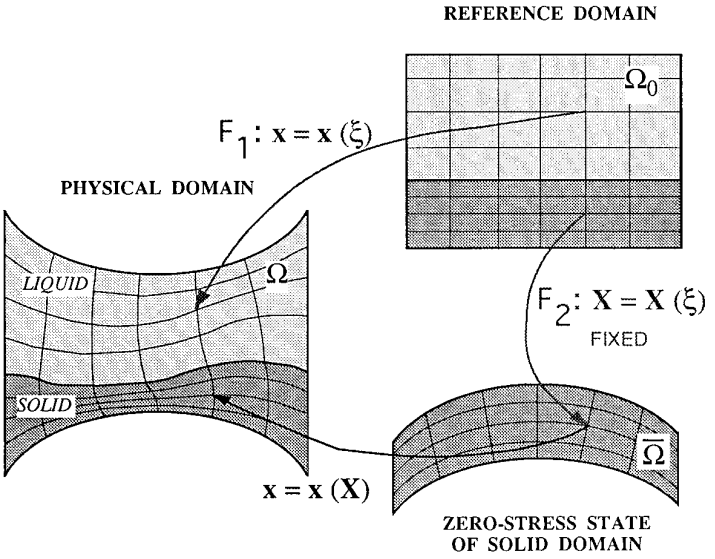

FIG. 4. Sketch of mappings from the liquid domain to the reference domain ($\Omega_L \to \Omega_0$); from the current solid configuration to the zero-stress state ($\Omega_S \to \overline{\Omega}$); and from the zero-stress state to the computational reference domain ($\overline{\Omega} \to \Omega_0$).

There are two distinct though coupled domains in the problem: one where the liquid flow occurs, which is mapped by the mesh generation equations to a reference domain where the Navier–Stokes system is solved; and the other where the roll cover deformation occurs, which is mapped to the stress-free domain where the equations of elasticity and the velocity field of the solid wall are solved. The difference is that the solution of the elasticity equations is itself the mapping, which therefore is not considered separately (see Fig. 4).

In summary, on the solid domain Ω_S, the deformation of the rubber is governed by the equilibrium equations together with the Mooney–Rivlin constitutive relation and the incompressibility constraint:

$$\nabla_X \cdot [-p^* \mathbf{F}^{-1} + \beta_0 \mathbf{F}^{\mathbf{T}} - \beta_1 (\mathrm{tr}(\mathbf{C}) \mathbf{F}^{\mathbf{T}} - \mathbf{C} \cdot \mathbf{F}^{\mathbf{T}})] = 0 \qquad \text{and} \qquad \det(\mathbf{F}) = 1. \tag{13}$$

The displacement vanishes at the interface where the rubber layer is attached to the rigid core of the roll (6) (cf. Fig. 2):

$$\mathbf{x} - \mathbf{X} = 0. \tag{14}$$

x and **X** are the coordinates in the laboratory frame of a material particle at the current and reference configuration, respectively.

At entrance and exit boundaries (5), the traction is set to zero, as a bald approximation:

$$\mathbf{N} \cdot \mathbf{T} = 0. \tag{15}$$

N is the unit normal vector to the entrance or exit of the reference domain, and **T** is the first Piola–Kirchhoff stress tensor.

At the interface between the liquid and solid domain (4), the no-slip/no-penetration condition and a force balance are applied:

$$\mathbf{v}_{\text{liq}} = \mathbf{v}_{\text{sol}} \qquad \text{and} \qquad \mathbf{N}\cdot\mathbf{T} = -\mathbf{n}\cdot\boldsymbol{\sigma}. \tag{16}$$

The parameters that govern this system are:

Dimensionless undeformed clearance (or interference): H_0/R

Reynolds Number: $Re \equiv \rho\overline{V}R/\mu$

Roll Speed Ratio: $S \equiv \omega_A/\omega_B$

Elasticity Number: $Es \equiv \mu\overline{V}/ER$

Dimensionless roll cover thickness: L/R.

ω_A and ω_B are the angular velocities of rolls A and B; $2H_0$ is either the clearance or the interference between the undeformed rolls; R is the roll radius; μ is the liquid viscosity; $\overline{V} = (V_A + V_B)/2 = (\omega_A + \omega_B)R/2$ is the average linear velocity of the roll surfaces, L is the thickness of the roll cover, and E is its elastic modulus. For a Mooney–Rivlin material, it is given by $E = 4(\beta_0 - \beta_1)$. The harder the roll cover, the smaller the elasticity number; in the limit of rigid rolls, the elasticity number is zero. In the spring model, the elastic modulus E and the deformable layer thickness L are lumped in a single parameter: the spring constant K. In this situation, a modified elasticity number, $Ne^* \equiv \mu\overline{V}/KR^2$ is useful. The analog of Ne^* for the plane strain formulation is simply the product of the elasticity number and the ratio of the rubber cover thickness to the roll radius: $Ne \equiv Es \times L/R = \mu\overline{V}L/ER^2$.

In the calculations presented here, the speed ratio S is kept constant and equal to unity. Positive and negative gaps, different roll cover hardnesses, i.e., elasticity numbers, and roll cover thicknesses are explored. The results show how the flow rate through the gap varies with these parameters, and how to relate the empirical spring constant K in the linear spring model to roll-cover properties, viz., elastic modulus and thickness.

The appropriate length scale in the direction transversal to the main flow is the actual distance between the two surfaces, that is unknown *a priori* and part of the solution. Even though all the results are presented in dimensionless variables, the equations that govern this situation were solved in their dimensional form.

3. SOLUTION METHOD

The system of partial differential equations presented in the previous section is solved by Galerkin's method with finite element basis functions, the basis function set being progressively increased (''refinement of the mesh'') until further increase changed the approximation to the ultimate solution less than the desired accuracy.

3.1. *Galerkin's Method*

The weighted residuals of Galerkin's method of solving partial differential equation systems amount to what is called the weak form of a system. A weighted residual of a differential equation is obtained by multiplying it by a "test" function and integrating the product over the domain. If the highest-order derivatives in the differential equation arise from the divergence operator operating on gradients, as in the momentum balances and equilibrium force balances above, applying the divergence theorem replaces the divergence operator by surface integrals in such a way that the basis functions used to represent the solution of the differential equation need not be continuously differentiable. In Galerkin's method, the unknown fields are represented by the same basis functions as are used as the weighting functions.

In the procedure followed here, the weighted residual equations defined over the liquid domain Ω_L have to be transformed to equivalent forms on the known (and fixed) reference domain Ω_0. This mapping is represented by $\mathscr{T}_1$ in Fig. 4. The Jacobian of $\mathscr{T}_1$ is denoted by $|\mathbf{J}|$,

$$|\mathbf{J}| \equiv \frac{\partial x}{\partial \xi}\frac{\partial y}{\partial \eta} - \frac{\partial y}{\partial \xi}\frac{\partial x}{\partial \eta}.$$

The resulting set of weighted residuals of the equations (x- and y-momentum, continuity, and x- and y-mapping) posed in the reference domain Ω_0 is

$$R_i^{M_x} = \int\int_{\Omega_0} \left\{ \mathrm{Re}\ \phi_i \left(u\frac{\partial u}{\partial x} + v\frac{\partial u}{\partial y} \right) + \frac{\partial \phi_i}{\partial x}\left(-p + 2\frac{\partial u}{\partial x} \right) + \frac{\partial \phi_i}{\partial y}\left(\frac{\partial u}{\partial y} + \frac{\partial v}{\partial x} \right) - St\, g_x \phi_i \right\} |\mathbf{J}|\, d\Omega_0 - \int_{\Gamma_0} \phi_i (\mathbf{n}\cdot\boldsymbol{\sigma})_x \left(\frac{d\Gamma}{d\Gamma_0} \right) d\Gamma_0 \tag{17a}$$

$$R_i^{M_y} = \int\int_{\Omega_0} \left\{ \mathrm{Re}\ \phi_i \left(u\frac{\partial v}{\partial x} + v\frac{\partial v}{\partial y} \right) + \frac{\partial \phi_i}{\partial x}\left(\frac{\partial u}{\partial y} + \frac{\partial v}{\partial x} \right) + \frac{\partial \phi_i}{\partial y}\left(-p + 2\frac{\partial v}{\partial y} \right) - St\, g_y \phi_i \right\} |\mathbf{J}|\, d\Omega_0 - \int_{\Gamma_0} \phi_i (\mathbf{n}\cdot\boldsymbol{\sigma})_y \left(\frac{d\Gamma}{d\Gamma_0} \right) d\Gamma_0 \tag{17b}$$

$$R_i^c = \int\int_{\Omega_0} \left(\frac{\partial u}{\partial x} + \frac{\partial v}{\partial y} \right) \chi_i |\mathbf{J}|\, d\Omega_0 \tag{17c}$$

$$R_i^x = -\int\int_{\Omega_0} D_\xi \left(\frac{\partial y}{\partial \eta}\frac{\partial \phi_i}{\partial x} - \frac{\partial x}{\partial \eta}\frac{\partial \phi_i}{\partial y} \right) d\Omega_0 + \int_{\Gamma_0} D_\xi \frac{1}{|\mathbf{J}|}\left(\frac{\partial y}{\partial \eta} n_x - \frac{\partial x}{\partial \eta} n_y \right) \phi_i \left(\frac{d\Gamma}{d\Gamma_0} \right) d\Gamma_0 \tag{17d}$$

$$R_i^y = -\int\int_{\Omega_0} D_\eta \left(-\frac{\partial y}{\partial \xi}\frac{\partial \phi_i}{\partial x} + \frac{\partial x}{\partial \xi}\frac{\partial \phi_i}{\partial y} \right) d\Omega_0 + \int_{\Gamma_0} D_\eta \frac{1}{|\mathbf{J}|}\left(-\frac{\partial y}{\partial \xi} n_x + \frac{\partial x}{\partial \xi} n_y \right) \phi_i \left(\frac{d\Gamma}{d\Gamma_0} \right) d\Gamma_0. \tag{17e}$$

The weighting functions ϕ_i associated with the momentum equations and mesh generation equations were bi-quadratic, and χ_i, related with the continuity equation was piecewise linear discontinuous.

When the spring model is used to describe the deformation of the roll cover, the force balance at the deformable wall represented by Eq. (5) is also applied in an integral way. There one of the residuals of the mesh generation equations is replaced by the weighted residual of the normal stress balance:

$$R_i^x = \int_{\Gamma_0} \left\{ \frac{1}{K} \mathbf{N}_0 \cdot (\mathbf{n} \cdot \boldsymbol{\sigma}) + \mathbf{N}_0 \cdot (\mathbf{x} - \mathbf{X}_0) \right\} \Phi_i \frac{d\Gamma_{dw}}{d\Gamma} d\Gamma = 0.$$

The weighting functions Φ_i are chosen to be displaced Dirac–delta functions, such that the residuals become

$$R_i^x = \left\{ \frac{1}{K} \mathbf{N}_0 \cdot (\mathbf{n} \cdot \boldsymbol{\sigma}) + \mathbf{N}_0 \cdot (\mathbf{x} - \mathbf{X}_0) \right\} \Big|_{\mathbf{x}_i} = 0. \tag{18}$$

When the plane-strain model is used, the velocity and deformation fields over the entire roll cover have to be calculated. The differential equations that describe these fields over the solid domain Ω_S are written in the *zero-stress* configuration $\overline{\Omega}$, which is fixed. From the numerical point of view, it is convenient to integrate the momentum residuals of both the liquid flow and the elasticity equations over the computational domain Ω_0. For that, a mapping $\mathbf{X} = \mathbf{X}(\boldsymbol{\xi})$ from Ω_0 to $\overline{\Omega}$ has to be constructed. It is represented by $\mathscr{T}_2$ in Fig. 4. Unlike $\mathscr{T}_1$, this mapping is known and it simply represents a change of domain of integration. The Jacobian of this transformation is denoted by $|\mathbf{J}^*|$.

The resulting set of weighted residuals of the equations of x-position and y-position, and incompressibility, in the reference domain Ω_0, is

$$R_i^x = -\int\int_{\Omega_0} \left[T_{xX} \frac{\partial \phi_i}{\partial X} + T_{xY} \frac{\partial \phi_i}{\partial X} \right] |\mathbf{J}^*| \, d\Omega_0 + \int_{\Gamma_0} \phi_i (\mathbf{N} \cdot \mathbf{T})_x \left(\frac{d\overline{\Gamma}}{d\Gamma_0} \right) d\Gamma_0 \tag{19a}$$

$$R_i^y = -\int\int_{\Omega_0} \left[T_{yX} \frac{\partial \phi_i}{\partial X} + T_{yY} \frac{\partial \phi_i}{\partial X} \right] |\mathbf{J}^*| \, d\Omega_0 + \int_{\Gamma_0} \phi_i (\mathbf{N} \cdot \mathbf{T})_y \left(\frac{d\overline{\Gamma}}{d\Gamma_0} \right) d\Gamma_0 \tag{19b}$$

$$R_i^{p^*} = \int\int_{\Omega_0} \left[\frac{\partial x}{\partial X} \frac{\partial y}{\partial Y} - \frac{\partial x}{\partial Y} \frac{\partial y}{\partial X} - 1 \right] \chi_i |\mathbf{J}^*| \, d\Omega_0. \tag{19c}$$

With the complete two-dimensional description, the force balance at the deformable wall represented by Eq. (16b) is applied as a natural boundary condition on Eqs. (19a) and (19b): The loading force acting on the elastic roll cover $\mathbf{N} \cdot \mathbf{T}$ that appears in the line integrals of the weighted residuals is replaced by the negative of the liquid traction $-\mathbf{n} \cdot \boldsymbol{\sigma}$ at the deformable wall. The weighting functions ϕ_i were bi-quadratic, and χ_i were piecewise linear discontinuous.

All of the integrals are evaluated by Gaussian quadrature with three Gauss points per element in each direction of integration [27].

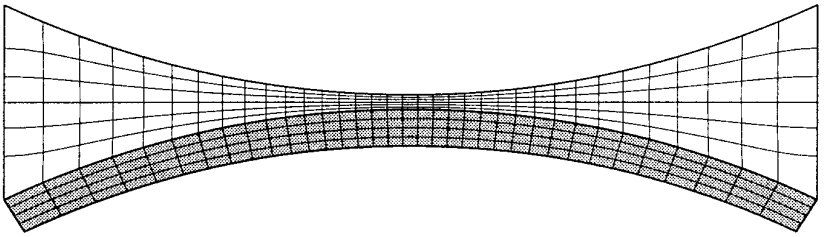

FIG. 5. Mesh of finite elements used with Galerkin's solution method: 350 elements and 7014 degrees of freedom.

3.2. *Solution of the Non-linear System*

Once the field variables are represented in terms of the basis functions, the system of partial differential equations, Eqs. (17) to (19), reduces to simultaneous algebraic equations for the coefficients of the basis functions of all the fields. This set of equations is non-linear and sparse. It is solved by Newton's method, which requires evaluation of the full Jacobian matrix, viz.,

$$\mathbf{u}_{(k+1)} = \mathbf{u}_{(k)} + \delta\mathbf{u}$$
$$\mathbf{J}(\delta\mathbf{u}) = -\mathbf{R}.$$

$\mathbf{u}$ is the vector of the unknown coefficients of the basis functions for the velocity, pressure, and nodal positions. $\mathbf{R}$ is the vector of weighted residuals, given by Eqs. (17) to (19), and $\mathbf{J}$ is the Jacobian matrix of sensitivities of the residuals to the unknowns, i.e.,

$$J_{ij} \equiv \frac{\partial R_i}{\partial u_j}.$$

The iteration proceeded until $\|\delta\mathbf{u}\|_{L_2} + \|\mathbf{R}\|_{L_2} < 10^{-7}$. At each Newton iteration, a linear system of equations was solved. The Jacobian matrix was factorized into a unit lower triangular matrix $\mathbf{L}$ and a unit upper triangular matrix $\mathbf{U}$ by a frontal solver.

Newton's method converges quadratically close to the solution. However, it can fail to converge if the initial guess is not close enough to the solution or if the solution does not exist for a given set of parameters. In order to improve the likelihood of convergence and to obtain solutions around turning points, a pseudo-arc-length continuation method was employed [28].

The domain of liquid flow was divided into 210 elements, and the domain of solid deformation (for the plane-strain model), into 140 elements.

The number of simultaneous equations when the spring model formulation was used was 4322, and when the plane strain model was used it was 7014. The additional equations governed the roll cover deformation and its velocity. A sample mesh for the plane-strain calculation is illustrated in Fig. 5. The dark region denotes the solid domain. The computations were made on a Cray X-MP.

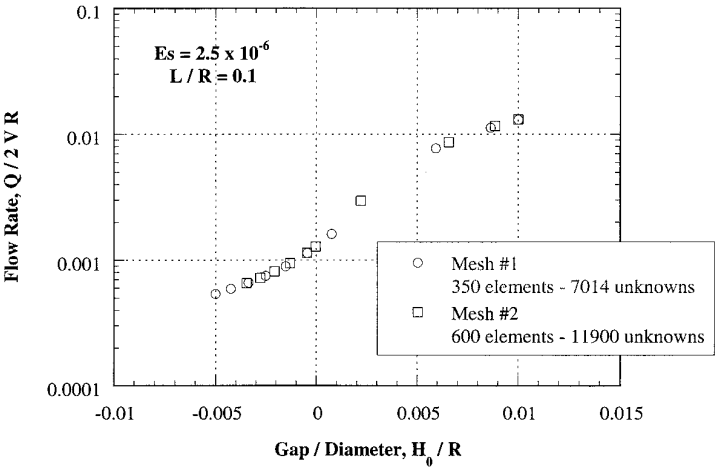

FIG. 6. Comparison of predicted flow rates with two different meshes: (a) 350 elements; (b) 600 elements. $Es = 2.5 \times 10^{-6}$ and $L/R = 0.1$.

Figure 6 illustrates the comparison of predicted flow rates with two different meshes: The one illustrated in Fig. 5 and used throughout this paper and a more refined one, that consisted of 600 elements, leading to a system of 11900 equations. The predicted flow rate was virtually insensitive to mesh refinement; it only changed in the fourth significant figure.

4. RESULTS AND DISCUSSIONS

4.1. *Predictions of Plane-Strain Model*

The flow through the deformable gap was evaluated at different clearances and interferences H_0/R, elasticity number $Es \equiv \mu\overline{V}/ER$, and roll cover thickness L/R.

Figure 7 shows the streamlines of the flow at different gaps (positive and negative) and elasticity number $Es = 2.5 \times 10^{-6}$ and thickness $L/R = 0.1$, i.e., $Ne \equiv Es \times L/R = \mu\overline{V}L/ER^2 = 2.5 \times 10^{-7}$. Flow states (a) and (b) have positive gaps, i.e., clearance between the undeformed surfaces; and flow states (c) and (d) have negative gaps, i.e., the roll surfaces would be in interference if they were rigid. If the rolls are far apart, the pressure that develops is not strong enough to deform the roll cover and the gap behaves as if it were rigid. As the rolls are pressed against each other, the pressure in the converging–diverging channel rises and the roll cover deforms more and more. At large interference (negative gaps), the liquid layer between the two rolls is so thin as to be almost imperceptible in the plots.

Figure 8 shows the dimensionless flow rate $q^* \equiv Q/2\overline{V}R$ at rubber cover thickness $L/R = 0.1$ versus elasticity number Es, and center-to-center position, characterized by H_0/R. At large enough positive gaps, the curves for different elasticity numbers merge into a single line that matches the rigid-roll predictions, because the liquid pressure is not high enough to deform the rubber cover. As the rolls are pushed together, the flow rate falls. At negative gaps, the flow rate sensitivity to roll position

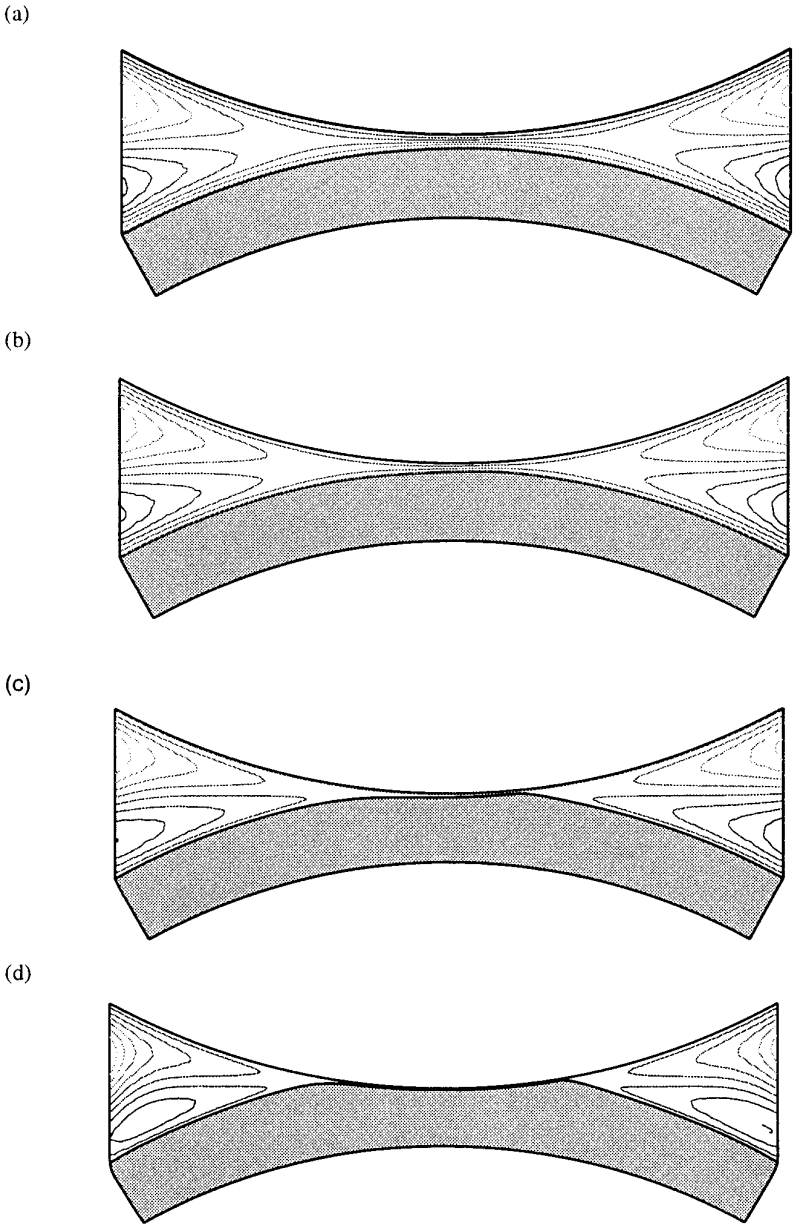

FIG. 7. Streamlines at $Es \times L/R = 2.5 \times 10^{-6}$, $L/R = 0.1$, and H_0/R: (a) = 10^{-2}; (b) = 6×10^{-3}; (c) = (—) 5×10^{-4}; and (d) = (—) 8×10^{-3}.

becomes relatively small. This is very important for roll coating operations. It means that the variation of the liquid layer thickness caused by roll run-out (out-of-roundness) is much smaller when a deformable roll is used and it diminishes as the rolls are pressed against each other. At a fixed center-to-center distance, the softer the roll, i.e., the larger the elasticity number, the larger the flow rate. The softer

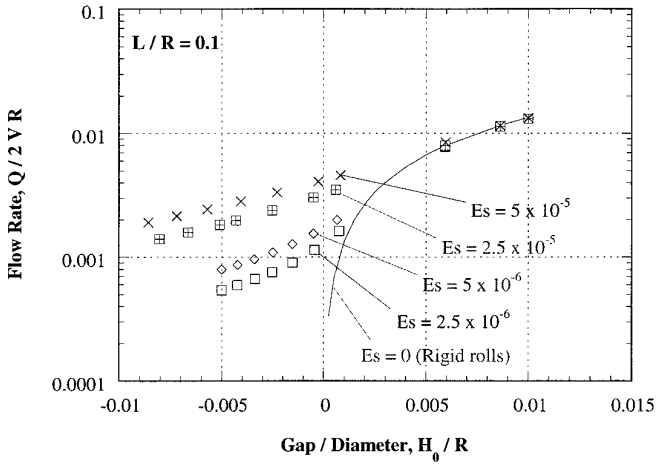

FIG. 8. Dimensionless flow rate predictions of the plane-strain model at different gaps (positive and negative) and elasticity numbers. $L/R = 0.1$. The continuous line represents the solution obtained with rigid rolls.

the roll, the more it deforms and, therefore, the higher the flow of liquid dragged through the gap.

As mentioned in Section 2, with the spring model the elastic modulus E of the roll cover and its thickness L are lumped in a single parameter: the spring constant K. The modified elasticity number is defined as $Ne^* \equiv \mu\overline{V}/KR^2$. The plane-strain model permits an analysis of the two parameters separately. Figure 9 shows the dimensionless flow rate as a function of center-to-center distance at roll cover thicknesses L/R from 0.02 up to 0.2 and different elasticity numbers Es, such that the modified elasticity number in all cases is $Ne \equiv Es \times L/R = 2.5 \times 10^{-7}$. The

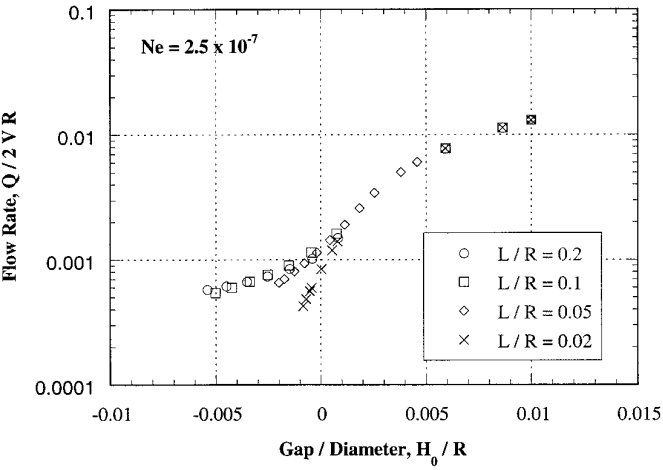

FIG. 9. Dimensionless flow rate predictions of the plane-strain model versus gap and roll cover thickness at modified elasticity number $Ne \equiv Es \times L/R = 2.5 \times 10^{-7}$.

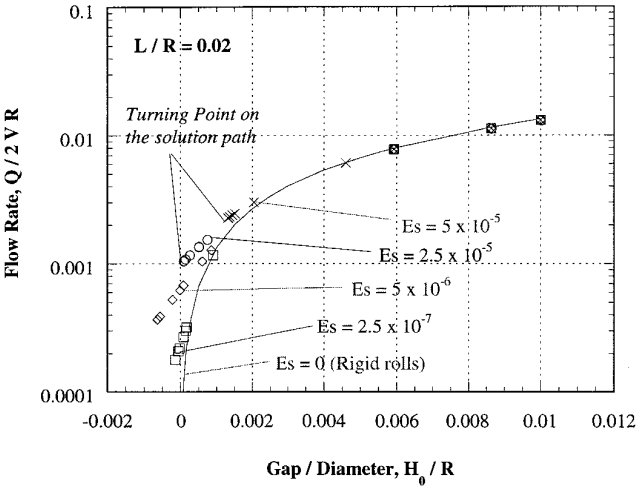

FIG. 10. Dimensionless flow rate predictions of the plane-strain model versus gap and elasticity number *Es*. $L/R = 0.02$.

flow rate predictions at the same modified elasticity number *Ne* vary with elasticity number *Es* and cover thickness. The thicker cover deforms more and yields larger flow rates. However, in the range of interference explored here (and commonly used in roll coating operations), the flow rate predictions are virtually the same for roll cover thickness larger than $L/R > 0.1$. These results illustrate a limitation of the spring model: the elastic modulus and thickness of roll cover cannot be combined in a single parameter if the roll cover thickness is smaller than $L/R < 0.1$. Fortunately the roll cover thickness encountered in roll coating applications are generally on the order of $L/R = 0.1$ (1 cm cover thickness in a 10 cm radius roll) or larger.

Figure 10 shows the dimensionless flow rate as a function of elasticity number and center-to-center distance at $L/R = 0.02$. For thin roll covers, the sensitivity of flow rate to roll position is much larger than for the case of thicker roll covers. At high elasticity numbers (soft roll), $Es = 2.5 \times 10^{-5}$ and 5×10^{-5} in Fig. 10, a turning point on the solution path occurs at $H_0/R = 8.6 \times 10^{-6}$ and $H_0/R = 1.3 \times 10^{-3}$, respectively. A steady-state solution could not be found beyond these values of center-to-center distance.

Turning points could also be detected at different roll cover thickness and elasticity numbers. Figure 11 illustrates the solution path at $Es = 2.5 \times 10^{-4}$ and $L/R = 0.1$. The rubber cover deforms even at a gap of $H_0/R = 0.01$ because it is very soft. As the rolls are pushed against each other, the roll cover deforms more and more and a small bump is formed downstream of the region of closest approach between the rolls. The bump is caused by the negative liquid pressure downstream of the center-to-center line, by the incompressibility condition on the rubber, and also by the shear force that the liquid exerts on the rubber layer. If the rolls are brought even closer, a turning point on the solution path occurs at approximately $H_0/R = 6.18 \times 10^{-3}$. The deformable roll profile at a flow state beyond the turning point exhibits an exaggerated bump and the solution is unstable. This behavior was not

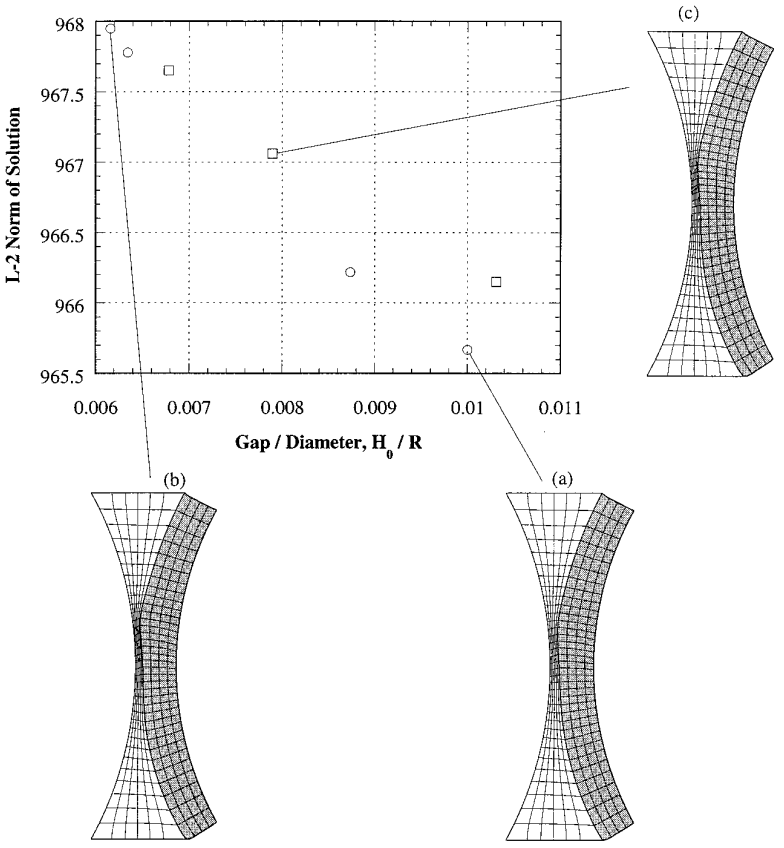

FIG. 11. Solution path with turning point at $Es = 2.5 \times 10^{-4}$ and $L/R = 0.1$. Deformable roll profiles at (a) $H_0/R = 10^{-2}$, (b) $H_0/R = 6.18 \times 10^{-3}$, and (c) $H_0/R = 7.9 \times 10^{-3}$.

and could not be predicted by the spring model, because that model accounts for neither the shear stress exerted by the liquid, nor the effects of incompressibility.

Because metering gaps can be controlled by loading rather than by setting the undeformed gap (load-controlled operation), it is useful to eliminate the latter and relate the flow rate Q directly to the loading force W. This relation is shown in Fig. 12 at $Ne = 2.5 \times 10^{-6}$. At the high load limit, the results can be fitted well to a power law:

$$Q \approx W^{-0.39}. \tag{20}$$

Coyle [14] reported an empirical fit of experimental data of wet thickness as a function of loading force. Although the experimental correlation was not dimensionally consistent, the flow rate dependence on loading force was approximately $Q \approx W^{-0.43}$.

4.2. *Predictions of the Spring Model*

The flow rate through the gap, the streamlines, and the profile of the deformable roll were evaluated from the solutions at different clearances (or interferences) and modified elasticity numbers $Ne^* \equiv \mu V/KR^2$.

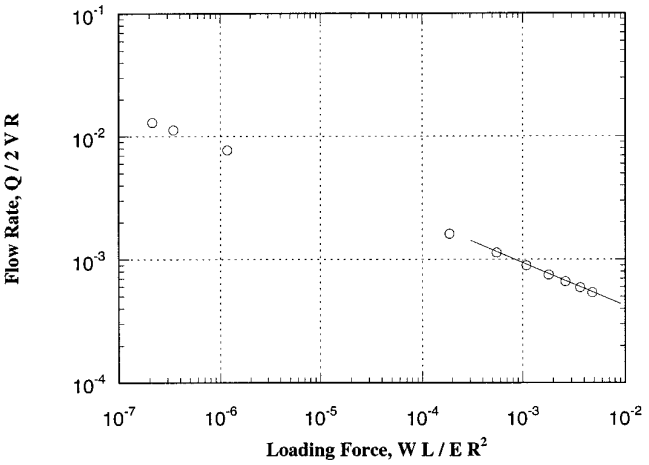

FIG. 12. Dimensionless flow rate predictions of plane-strain model at different loading at $Ne = 2.5 \times 10^{-7}$. The line represents the power-law fit $Q \approx W^{-0.39}$ at high loading force.

The streamlines of a series of flows at a modified elasticity number $Ne^* \equiv \mu V/KR^2$ of 10^{-7} and different center-to-center distances are shown in Fig. 13. Flow states (a) and (b) have positive gaps, i.e., clearance between the undeformed surfaces; state (c) has zero clearance, i.e., the distance between the centers of the rolls is exactly equal to the sum of the roll radii; and state (d) has a negative gap, i.e., the roll surfaces would be in interference if they were rigid.

The profile of the deformable roll is shown in Fig. 14 as a function of gap and modified elasticity number. At a given gap, the larger the elasticity number, i.e., the softer the roll, the wider is the distance between the rolls, as expected. At interference (negative gaps), an almost uniform channel is formed between the rolls.

The dimensionless flow rate $q^* \equiv Q/2VR$ is plotted versus gap (positive and negative) and modified elasticity number in Fig. 15. The trends are similar to those of the complete two-dimensional description: (1) At large enough gaps, all curves merge into the rigid roll prediction; (2) at a fixed gap, the softer the roll (higher elasticity number), the larger the flow rate; and (3) as the rolls are pressed against each other, the sensitivity of flow rate to gap diminishes.

Figure 16 illustrates the variation of the flow rate with loading force between the rolls at $Ne^* = 10^{-7}$. At the high load limit, the results can also be fitted to a power law:

$$Q \approx W^{-0.34}. \tag{21}$$

Both theoretical predictions reported here (Eqs. 20 and 21), for plane strain and spring model, agree qualitatively with the experiments; but the plate strain model gives a better quantitative agreement.

4.3. *Evaluation of the Empirical Spring Constant K*

The theoretical predictions presented in the previous section already illustrate limitation of the spring model, viz., for thin cover thickness, i.e., $L/R < 0.1$, the

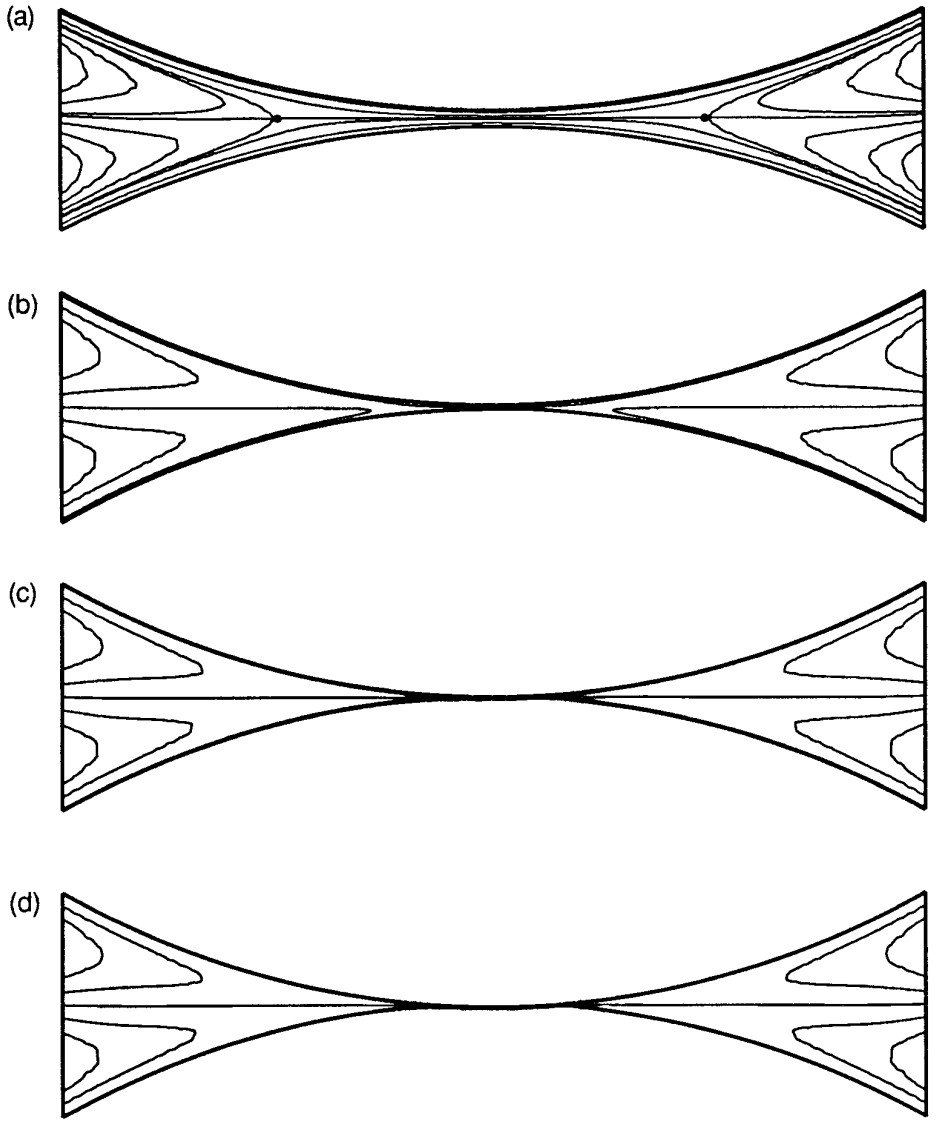

FIG. 13. Streamlines at $Ne^* = 10^{-7}$ and H_0/R: (a) = 10^{-1}; (b) = 2×10^{-3}; (c) = 0; and (d) = (—) 2×10^{-3}. The rolls are moving from left to right.

elastic modulus and roll cover thickness cannot be combined in a single parameter. However, most deformable rolls are in the range at which the approximation is valid.

The calculations with the simplified approach are much cheaper (in memory and in time) than the complete two-dimensional description of the roll cover deformation. With the spring model, the average time to perform each step of the Newton iteration was approximately 4 seconds; with the plane-strain model, the average time increased to approximately 20 seconds. Therefore, depending on the desired compromise between accuracy and cost, the spring model can be a valuable alterna-

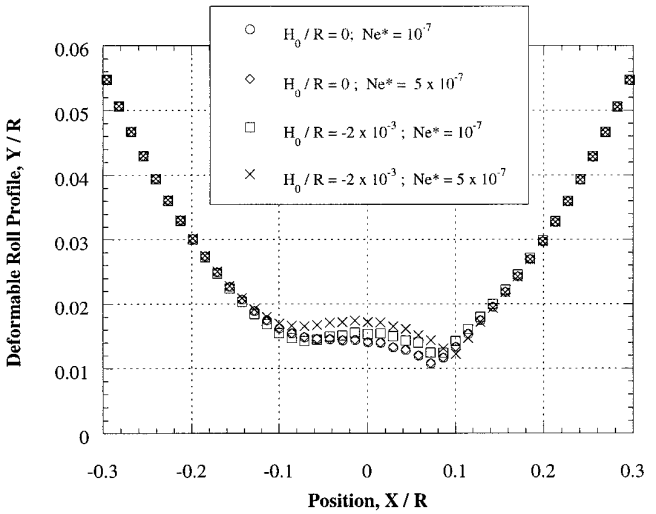

FIG. 14. Deformable roll profiles at different modified elasticity numbers *Ne** and undeformed gaps H_0/R. At a given gap, the softer the roll, the wider the distance between the rolls' surfaces.

tive for describing the roll cover deformation. In order to use this simplified approach, it is important to relate the empirical spring constant K to the properties of an incompressible roll cover: elastic modulus E and thickness L. As mentioned before, the relation proposed by Johnson [6] cannot be used, because most roll cover materials are nearly incompressible.

For the purpose of comparison, the modified elasticity number *Ne** is redefined as

$$Ne^* \equiv \frac{\mu \overline{V}}{K_{eq} R^2}.$$

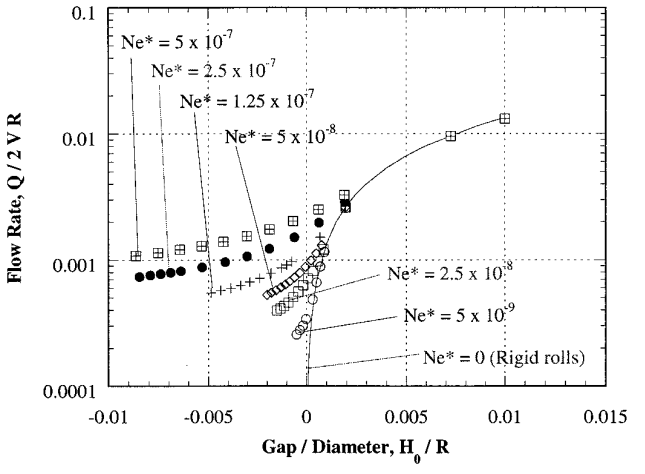

FIG. 15. Predicted dimensionless flow rate according to the spring model, versus gap (positive and negatives) and modified elasticity number *Ne**. The continuous line represents the states previously found in the case of rigid rolls.

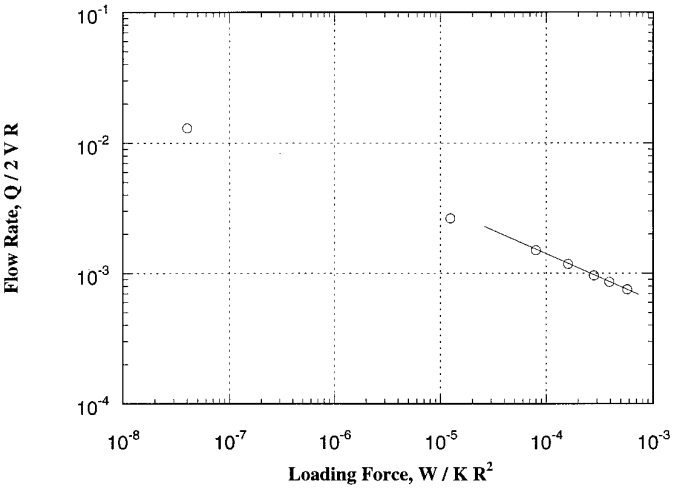

FIG. 16. Dimensionless flow rate predictions of spring model at different loading force at $Ne^* = 10^{-7}$. The line represents the power-law fit $Q \approx W^{-0.34}$ at high loading force.

For the plane strain model, K_{eq} is assumed to be proportional to the ratio of elastic modulus and roll cover thickness, i.e., $K_{eq} = \alpha E/L$. For the spring model K_{eq} is simply the spring constant K.

Figure 17 shows the dimensionless flow rate $q^* \equiv Q/2VR$ at a gap clearance of $H_0/R = -10^{-3}$ (negative gap), roll cover thickness $L/R = 0.1$, and different modified elasticity numbers Ne^* predicted by the spring and the plane-strain models. If $\alpha = 1$, i.e., $K_{eq} = E/L$, the spring model overpredicts the flow rate at all values of Ne^*. However, if α is set arbitrarily equal to 2, i.e., $K_{eq} = 2E/L$, the flow rates predicted

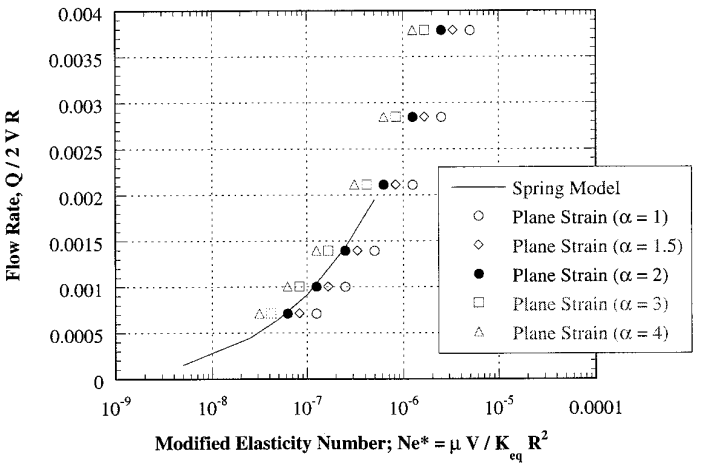

FIG. 17. Comparison of the dimensionless flow rate q^* versus modified elasticity numbers at $H_0/R =$ (—) 10^{-3} as predicted by the spring and plane-strain models of the roll cover. For the spring model $Ne^* = \mu\overline{V}/KR^2$. For the plane-strain model $Ne^* = \mu\overline{V}L/\alpha ER^2$.

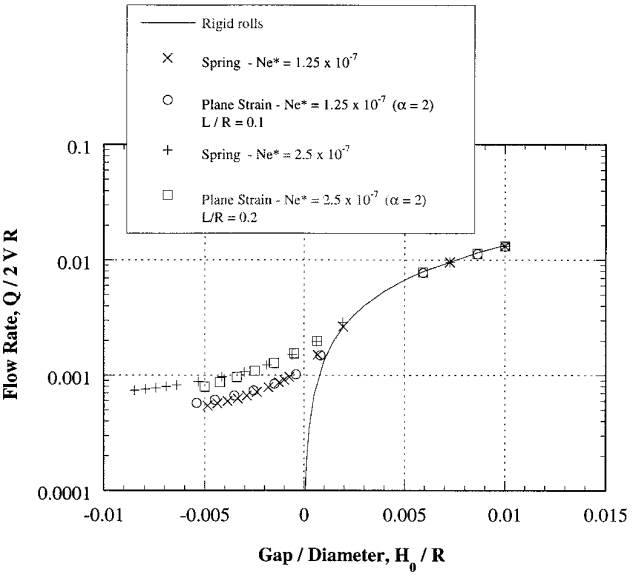

FIG. 18. Comparison of the dimensionless flow rate q^* versus gaps at $Ne^* = 1.25 \times 10^{-7}$, as predicted by the spring and plane-strain models of the roll cover.

by the spring formulation almost coincide with the ones yielded by the complete non-linear, plane-strain elasticity formulation. Therefore, the constant K in the spring model should be set equal to twice Young's modulus divided by the cover thickness:

$$K = 2 \times E/L.$$

To check if this approximation is still valid at different gaps and roll cover thicknesses, Fig. 18 compares the dimensionless flow rates q^* predicted by the two deformation models, as functions of center-to-center distance H_0/R at modified elasticity numbers $Ne^* = 1.25 \times 10^{-7}$ and 2.5×10^{-7}. The predictions of the plane-strain model were at $L/R = 0.1$ and $L/R = 0.2$, respectively, and are for $K_{eq} = 2 \times E/L$. The predicted flow rate between the two models is very close at the entire range of gaps examined.

Figures 17 and 18 illustrate that although much simpler, the spring model can predict flow rates close to those from the more complete plane-strain model if the appropriate spring constant is used.

Up to this point, only flow rates have been compared. Figure 19 shows the deformable roll profiles at $H_0/R = (-)2 \times 10^{-3}$ and $Ne^* = 5 \times 10^{-7}$ as predicted by the spring and plane-strain models. Again, the spring constant was set to $K = 2 \times E/L$. The predicted roll profiles are close. However, the elongated and almost uniform gap formed between the rolls is slightly larger when the plane-strain model is used, as expected. The main reason for that is the incompressibility of the roll cover.

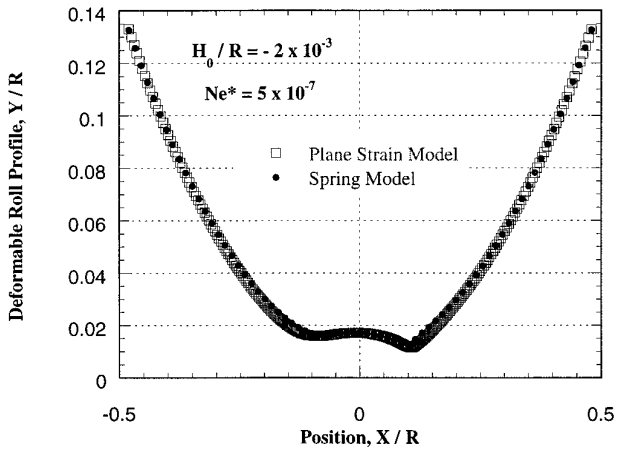

FIG. 19. Deformable roll profiles predicted by the spring and plane-strain models at H_0/R = (—) 2×10^{-3} and $Ne = 5 \times 10^{-7}$.

The main shortcoming of the spring model is that the velocity distribution it predicts along the surface of the deformable roll differs greatly from the one predicted with the plane-strain formulation, as depicted in Fig. 20. With the spring model, the velocity distribution is almost uniform along the resilient roll. When the plane-strain formulation is used, the velocity of the roll varies substantially along the roll surface. At the conditions shown in the plot, the surface velocity at the plane of the two roll centers ($X/R = 0$) is 10% larger than what it would be if the roll were rigid. This variation of the surface velocity is caused by the azimuthal deformation due to the incompressibility of the cover, which cannot be described by the simple spring model. Even though both rolls have the same angular speed, the velocity ratio at the center-to-center plane was 1.1. This velocity ratio can lead

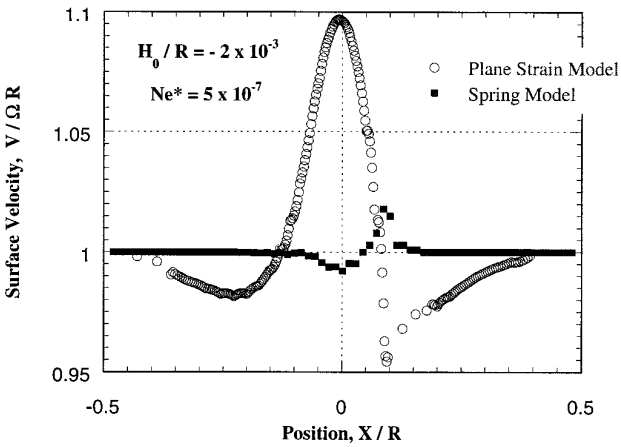

FIG. 20. Velocity distribution along the deformable wall predicted by the spring model and the plane-strain model.

to important differences in the amount of liquid carried out by each roll in the case of a forward film split flow.

5. FINAL REMARKS

Flow between a rigid and a deformable roll was analyzed. The viscous liquid flow and the elastic deformation of the roll cover are coupled, which constitutes an elastohydrodynamic action.

A complete two-dimensional formulation of the situation was used for both the liquid flow and for the elastic roll cover. The liquid flow between the rotating rolls was described by the Navier–Stokes system of equations. The deformation of the compliant roll cover was described by a plane-strain model of incompressible Mooney–Rivlin material (non-linear elasticity). The approximate and computationally cheaper approach, which consisted of a series of independent radial springs to describe the roll cover deformation, was also explored. The merits and disadvantages of both deformation descriptions were discussed. The results reveal the range of parameters at which the spring model provides a good approximation and the relation between the empirical spring constant to the roll cover properties (thickness and elastic modulus).

The resulting system of partial differential equations was solved by Galerkin's method and finite element basis functions. Newton's method was used to solve the non-linear set of algebraic equations obtained by discretization of the problem. With this fully coupled approach, convergence was achieved in four to five iterations, provided a good initial guess was employed at each condition. This was accomplished by using pseudo-arc-length continuation strategy, which also permitted the computation of solutions around turning points.

The theoretical predictions reveal how the flow rate varies with the roll cover hardness and the center-to-center distance. The results illustrate how a deformable roll can be used to obtain thin coated layers with much less sensitivity to roll runout than those obtained with rigid rolls.

ACKNOWLEDGMENTS

M. S. Carvalho was supported by a fellowship from CAPES (Departament of Education, Federal Government of Brazil). Further support came from cooperating corporations through the Center for Interfacial Engineering and was supplemented by the National Science Foundation and the Minnesota Supercomputer Institute.

REFERENCES

1. D. J. Coyle, C. W. Macosko, and L. E. Scriven, *J. Fluid Mech.* **171,** 183 (1986).
2. D. F. Benjamin, T. J. Anderson, and L. E. Scriven, *AIChE J.* **41,** 1045 (1995).
3. P. H. Gaskell, M. D. Savage, J. L. Summers, and H. M. Thompson, *J. Fluid Mech.* **298,** 113 (1995).
4. D. Dowson and G. R. Higginson, *Elastohydrodynamic Lubrication* (Pergamon, Oxford, 1966).
5. A. Bennet and G. R. Higginson, *J. Mech. Eng. Sci.* **12,** No. 3, 218 (1970).
6. K. L. Johnson, *Contact Mechanics* (Cambridge Univ. Press, Cambridge, UK, 1985).

7. C. J. Hooke, *Wear.* **111,** 83 (1986).
8. P. Meijers, *Appl. Sci. Res.* **18,** 353 (1968).
9. D. Dowson and Z. Jin, in *Proceedings of the 16th Leeds–Lyon Symposium on Tribology, Lyon, France, 1989,* p. 263.
10. R. C. Batra, *J. Appl. Mech.* **47,** 82 (1980).
11. C. N. Bapat and R. C. Batra, *Int. J. Numer. Methods Eng.* **20,** 1911 (1984).
12. J. T. Oden and T. L. Lin, *Comput. Methods Appl. Mech. Eng.* **57,** 297 (1986).
13. D. J. Coyle, *Chem. Eng. Sci.* **43,** 2673 (1988).
14. D. J. Coyle, Forward roll coating with deformable rolls, in *Proceedings, AIChE Spring National Meeting, 1988,* Paper 3b.
15. M. S. Carvalho and L. E. Scriven, *TAPPI J.* **77,** No. 5, 201 (1994).
16. M. S. Carvalho and L. E. Scriven, in *First European Coating Symposium, 1995,* pp. 221.
17. M. S. Carvalho and L. E. Scriven, in *First European Coating Symposium, 1995,* p. 75.
18. S. F. Kistler and L. E. Scriven, Coating flows, in *Computational Analysis of Polymer Processing,* edited by J. R. A. Pearson and S. M. Richardson (Applied Science Publishers, London/New York, 1983), p. 243.
19. S. F. Kistler and L. E. Scriven, *Int. J. Numer. Methods Fluids* **4,** 207 (1984).
20. K. N. Christodoulou and L. E. Scriven, *J. Comput. Phys.* **99,** 39 (1990).
21. P. A. Sackinger, P. R. Schunk, and R. R. Rao, *J. Comput. Phys.* **125,** 83 (1996).
22. J. F. Thompson, Z. Warsi, and C. W. Mastin, *Numerical Grid Generation, Foundations and Applications* (North-Holland, New York, 1985).
23. J. E. Castillo, *Mathematical Aspects of Numerical Grid Generation* (SIAM, Philadelphia, 1991).
24. P. M. Knupp and S. Steinberg, *The Fundamentals of Grid Generation* (CRC Press, New York, 1993).
25. J. M. de Santos, *Two-Phase Cocurrent Downflow through Constricted Passages,* Ph.D. thesis, (University of Minnesota, Minneapolis, 1991).
26. M. E. Gurtin, *Introduction to Continuum Mechanics* (Academic Press, New York, 1981).
27. V. F. de Almeida, *Gas–Liquid Counter Flow in Constricted Passages,* Ph.D. thesis (University of Minnesota, Minneapolis, 1995).
28. T. J. R. Hughes, *The Finite Element Method: Linear Static and Dynamic Finite Element Analysis* (Prentice Hall, Englewood Cliffs, NJ, 1987).
29. J. H. Bolstad and H. B. Keller, *SIAM J. Sci. Stat. Comput.* **7,** 1081 (1986).